Proceedings of Engineering and Technology Innovation, vol. 28, 2024, pp. 15-29

Marine Characteristic Changes Associated with Typhoon Soulik Observed Using Wave and Underwater Gliders

Jong-Wu Hyeon, Dae-Hyeong Ji, Seom-Kyu Jung, Sung-Hyub Ko*

Marine Domain & Security Research Department, Korea Institute of Ocean Science & Technology, Busan, Korea

Received 19 May 2024; received in revised form 04 August 2024; accepted 05 September 2024

DOI: https://doi.org/10.46604/peti.2024.13747

Abstract

To assess the impact of Typhoon Soulik on the marine environment, unmanned platforms, specifically wave and underwater gliders, are used for surveys in the East Sea. From August 20 to 30, 2018, the wave glider collected meteorological data, while the underwater glider conducts CTD measurements within the typhoon's impact zone. The data are compared with marine buoy data from the Korea Meteorological Administration and forecast model outputs using RMSE and correlation coefficients to evaluate the characteristics of each data source. The unmanned platform effectively capture the marine environmental changes during the typhoon passage, and the forecast model results show relatively lower RMSE and correlation with the observed data. The study also determines the time required for conditions to revert to pre-typhoon states. This research demonstrates the potential of unmanned platform data for enhancing marine surveys and forecast model accuracy.

Keywords: Soulik, underwater glider, wave glider, marine buoy, forecast model

1. Introduction

Oceanographic surveys traditionally rely on ships, buoys, and observatories, but recent advancements in unmanned observation technology have led to the autonomous conduct of ocean surveys. These advancements include unmanned surface vehicles (USVs) and unmanned underwater vehicles (UUVs). Among these, the wave glider [1-3] stands out as a USV propelled by wave energy, equipped with various observation and communication instruments tailored to its deployment location. Typically, the wave glider gathers meteorological (e.g., air temperature, air pressure, wind) and oceanographic (e.g., water temperature, wave height) data, with the flexibility to incorporate additional sensors [4-6]. For instance, Moh et al. [7] deployed an acoustic doppler current profiler (ADCP), fluorometer, and conductivity, temperature, and depth (CTD) sensor to conduct an ocean survey near Jeju Island, South Korea, over a 985 km track. Their study delineated water dilution patterns and elucidated the relationship between turbidity and mixed layer depth across the surveyed area.

Similarly, Wiggins et al. [8] conducted marine mammal passive monitoring surveys using a wave glider equipped with a high-frequency acoustic recording package in Hawaii, capturing dolphin vocalizations and humpback whale songs. Notably, the wave glider's capacity for unrestricted temporal and spatial operation enables it to traverse vast oceanic expanses [9] and monitor natural phenomena such as typhoons [10]. Conversely, the underwater glider [11-14], a type of UUV propelled by buoyancy control mechanisms rather than conventional propulsion systems, primarily measures water properties like temperature, salinity, and depth. While similar to Argo floats in operation, underwater gliders possess independent steering capabilities, facilitating precise navigation to designated locations. Recent developments in underwater glider technology,

* Corresponding author. E-mail address: kosh@kiost.ac.kr

English language proofreader: Chih-Wen Teng

notably the introduction of hybrid-type models equipped with propellers, have spurred research focusing on precision control. Nguyen et al. [15] proposed a depth control algorithm for hybrid underwater gliders, enabling precise depth navigation at constant cruising speeds, validated through MATLAB simulations.

Motivated by the capabilities of these unmanned platforms, this study utilizes both wave and underwater gliders to assess changes in the marine environment within the East Sea of South Korea following typhoon Soulik. Subsequent sections delineate the methodology, deployment procedures, and data analysis, offering a comprehensive evaluation of the typhoon's impact on oceanographic conditions in the study area.

2. Materials and Methods

On August 16, 2018, typhoon Soulik, initially located approximately 260 km northwest of Guam, progressed towards South Korea. By August 21, it approached the sea southeast of Jeju, eventually landing on August 23 and exiting to the East Sea by August 24. The typhoon dissipated around 480 km northeast of Dokdo after lasting approximately 210 hours [16]. Based on the predicted trajectory of the typhoon, the survey areas for unmanned platforms such as wave gliders and underwater gliders were determined, and oceanographic surveys were conducted within the influence of the typhoon.

2.1. Unmanned observation system

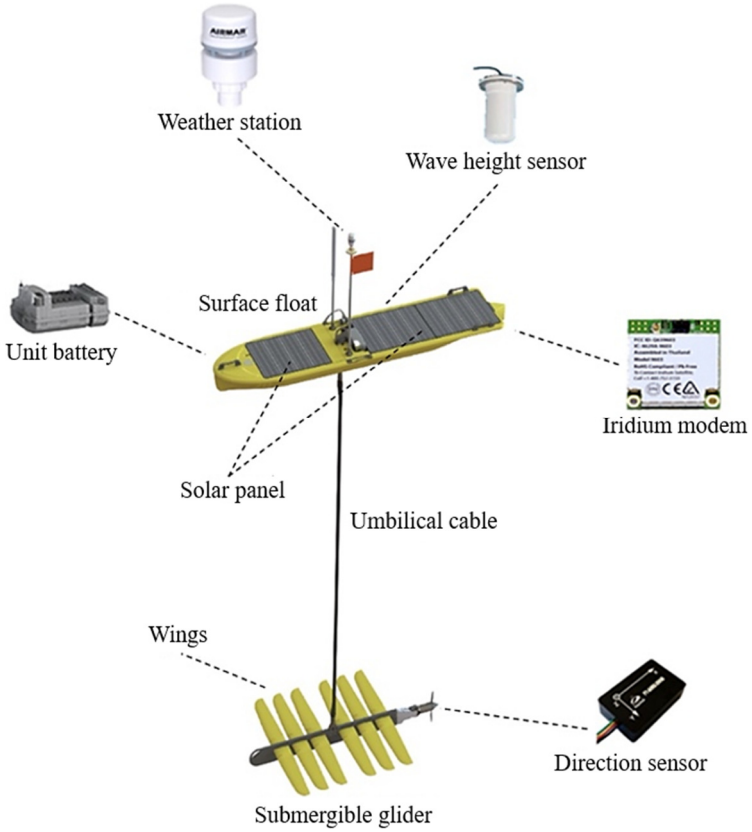

Fig. 1 Schematic of the wave glider

The wave glider comprises a surface float, a submersible glider, and an umbilical cable, as illustrated in Fig. 1. The surface float is versatile, accommodating various equipment types. Meteorological and oceanographic observations are collected using a weather station measuring air temperature, air pressure, wind speed, wind direction, and a wave height sensor installed on the surface float. The wave glider employs different communication techniques, such as radio frequency (RF), code division multiple access (CDMA), and iridium satellite communications, depending on signal strength. The observation and communication equipment on the surface float is powered by a built-in battery charged through a solar panel. Oscillatory movements of waves are converted into forward propulsion by the wings on the submersible glider's body. To adjust its

direction, the wave glider is equipped with an orientation sensor and rudder at its rear. The wave glider typically operates at an average speed of 1.8 knots and can achieve a maximum speed of about 3 knots under optimal conditions. These speeds are influenced by environmental factors and mission-specific configurations [17].

The Slocum G2 underwater glider [18-19], shown in Fig. 2, was made by Teledyne Webb Research. This glider has three parts: the front has a buoyancy engine, battery pack, and posture control device; the middle has a wing and a payload with a Seabird CTD sensor, profiler, and controller; and the back has the main computer, battery pack, air bladder, antenna, rudder, and power switch. The main computer includes modules like a motor driver, GPS receiver, communication module, motion sensor, and gyro sensor.

(a) Slocum G2

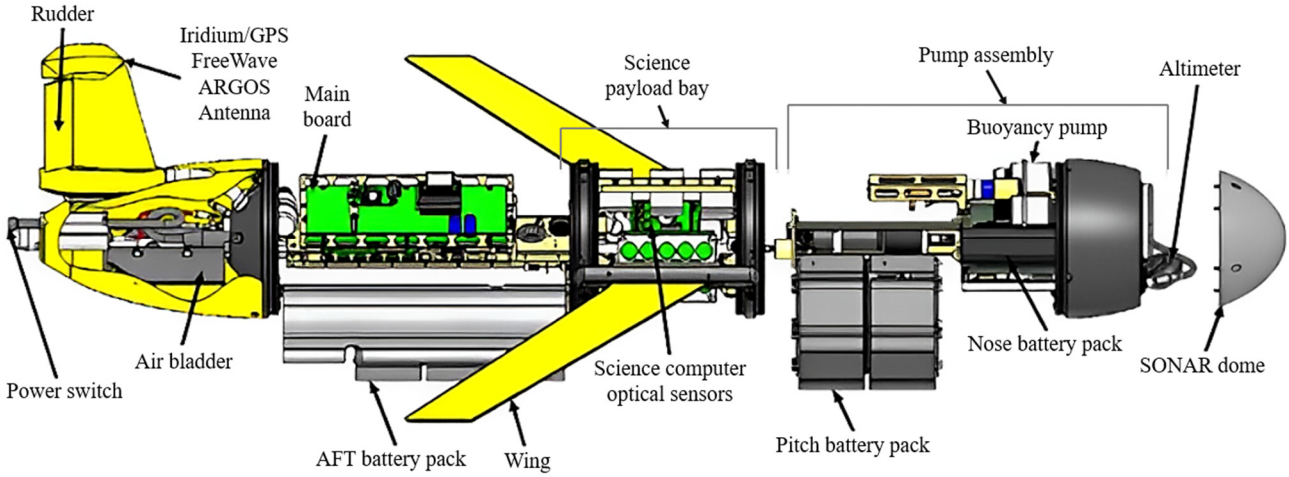

(b) Schematic of the Slocum G2

Fig. 2 Photograph of Slocum G2 underwater glider

The glider moves without a motor, using buoyancy and posture control along with steering. The glider moves by rocking up to 200 m deep, following changes in buoyancy and gravity. It can run for about a month with its built-in battery, covering 600-1,500 km at an average speed of 0.4-0.6 m/s. Real-time monitoring is possible with iridium satellite communication. Fig. 3 shows a schematic of a wave glider and an underwater glider doing an ocean survey. They were controlled separately with different software, giving instructions to the equipment and checking data and equipment status in real time. The specifications related to the wave and underwater glider are summarized in Table 1.

Table 1 Specifications of wave and underwater gliders

	Wave glider	Underwater glider
Model	Wave glider SV3	Slocum G2
Manufacturer	Liquid Robotics Inc.	Teledyne Webb Research
Dimensions	Surface float: 305 cm × 81 cm × 23 cm Submergible glider: 213 cm × 142 cm × 21 cm	Length: 1.5 m Hull diameter: 0.22 m

Table 1 Specifications of wave and underwater gliders (continued)

	Wave glider	Underwater glider
Weight	150 kg	54 kg
Battery life	Up to 1 year at sea	15-50 days (Alkaline) 4-12 months (Lithium)
Operation depth	Surface operation	Up to 200 m
Communication	RF, CDMA, Iridium	RF, Iridium, Argos
Speed	Average: 1.8 kts Max: 3 kts	Average: 0.68 kts Max: 1kts
Sensors	Weather station (Airmar Technology/PB200WX)	CTD (Sea-Bird Scientific/SLOCUMGLIDERCTD)

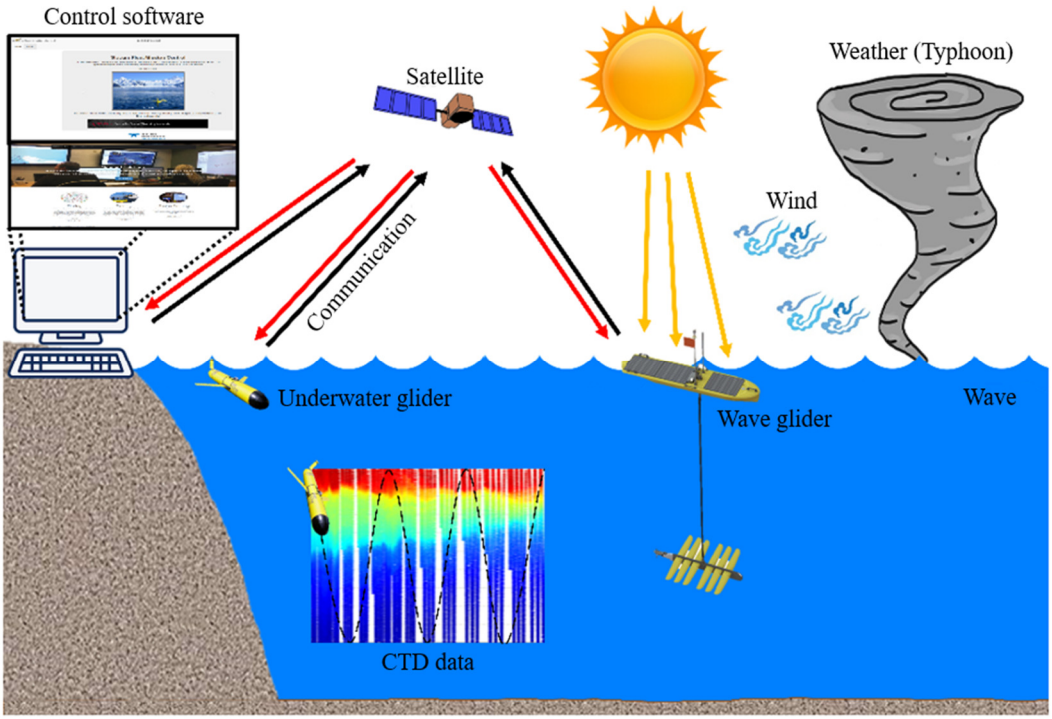

Fig. 3 Schematic of the unmanned observation system

2.2. *Survey area*

In Fig. 4, the expected typhoon path of August 18 is shown. The typhoon's path, locations, and radius of 30-knot winds (R30) are marked by green diamonds, lines, and circles. The survey area and Korea Meteorological Administration (KMA) marine buoys are in red dashed boxes and red diamonds. To avoid navigational hazards such as scattered nets and fishing gear along the East Sea coast, a survey area was selected between Samcheok and Ulleungdo, guided by ship schedules and the predicted typhoon path. The wave and underwater gliders were launched from Samcheok and Ulleungdo, respectively, with waypoints based on the typhoon's path. The marine buoys [20-21] operated by the KMA serve as marine meteorological observatories (Fig. 5). The Donghae and Ulleung marine buoys record hourly measurements of wind direction, speed, air pressure, temperature, humidity, wave height, period, direction, and water temperature.

Data are accessible on the KMA's official website (http://www.kma.go.kr/index.jsp). The Pacific Islands Ocean Observing System (PacIOOS) and Hybrid Coordinate Ocean Model (HyCOM) forecast models were selected to compare weather and CTD data, respectively. PacIOOS [22], part of the U.S. Integrated Ocean Observing System, generates forecast model results for up to 7 days from observation data recorded and statistically processed at 1 to 3-hour intervals, with coverage over a 0.5° by 0.5° longitude-latitude grid. HyCOM [23] is operated by institutions such as the National Oceanic and Atmospheric Administration (NOAA), the U.S. Naval Research Laboratory (NRL), and various research universities, and utilizes a hybrid vertical coordinate system for accurate ocean simulations. It processes real-time data from satellites, buoys,

and ships, incorporating data assimilation techniques to enhance prediction accuracy. HyCOM provides forecasts ranging from 1 to 7 days for short-term predictions and up to 2 weeks or more for medium- to long-term forecasts, covering a grid mesh of 0.08° by 0.08° in longitude and latitude.

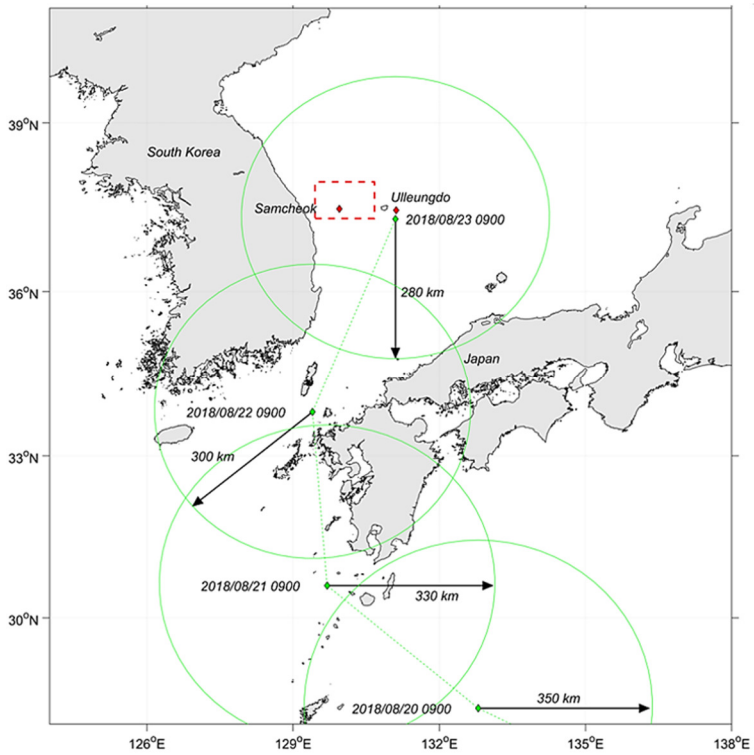

Fig. 4 The expected path of typhoon Soulik

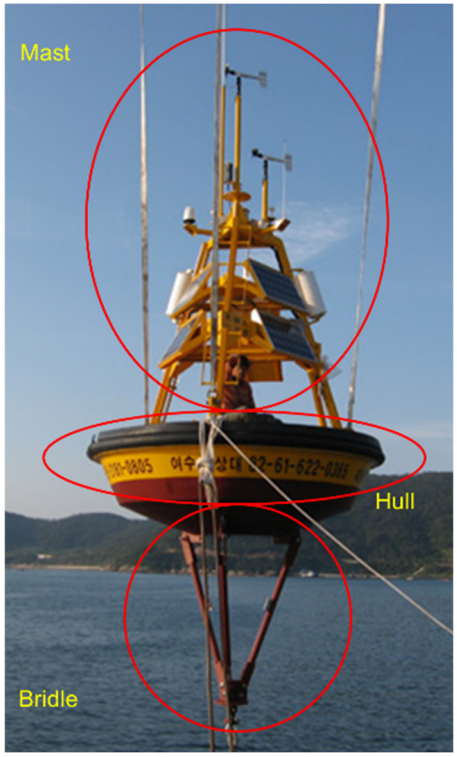

Fig. 5 Photograph of the marine buoy

3. Results

From August 20 to 30, 2018, the wave and underwater gliders conducted oceanographic surveys along the waypoints established within the survey area. The wave glider recorded meteorological data at 10-minute intervals, and the underwater glider collected CTD profiles at 1-meter increments up to 200 m depth. Firstly, the surveys were assessed to determine if the observations were made within the typhoon's influence based on the actual typhoon path. Following this assessment, time-series data from the wave glider were compared with measurements from marine buoys and forecast outputs from the PacIOOS model, and time-series data from the underwater glider were compared with forecast results from the HyCOM model.

3.1. Trajectory of the typhoon, unmanned platform

Fig. 6 provides an overview of the survey area, including data for the typhoon, wave glider, and underwater glider. Fig. 6 shows the following: the position of the typhoon center, trajectory, and R30 of the actual typhoon (black diamonds, dashed line, and circles); the position of the typhoon center, trajectory, and expected R30 area (green diamonds, dashed line, and circle); the time (UTC); the survey area (red dashed box); wave glider waypoints and trajectory (yellow diamonds and line); and underwater glider waypoints and trajectory (blue diamonds and line). The two red diamonds represent the marine buoys, with Donghae on the left side and Ulleung on the right side. According to data from the Donghae marine buoy, when the typhoon reached the survey area and dissipated, the average and maximum wind speeds were 5.4 and 14.1 m/s, respectively.

The R30 associated with the actual typhoon had a radius of at least 120 km, covering a large area over the East Sea of South Korea, including Ulleungdo. As shown in Fig. 6, the survey area was situated within the region where the R30 of both the expected and actual typhoons overlapped. Although the typhoon did not follow the predicted path, the R30, based on the forecasted trajectory, covered the pre-established observation area. This ensured that the two unmanned platforms were able to conduct the ocean survey within the typhoon's impact zone.

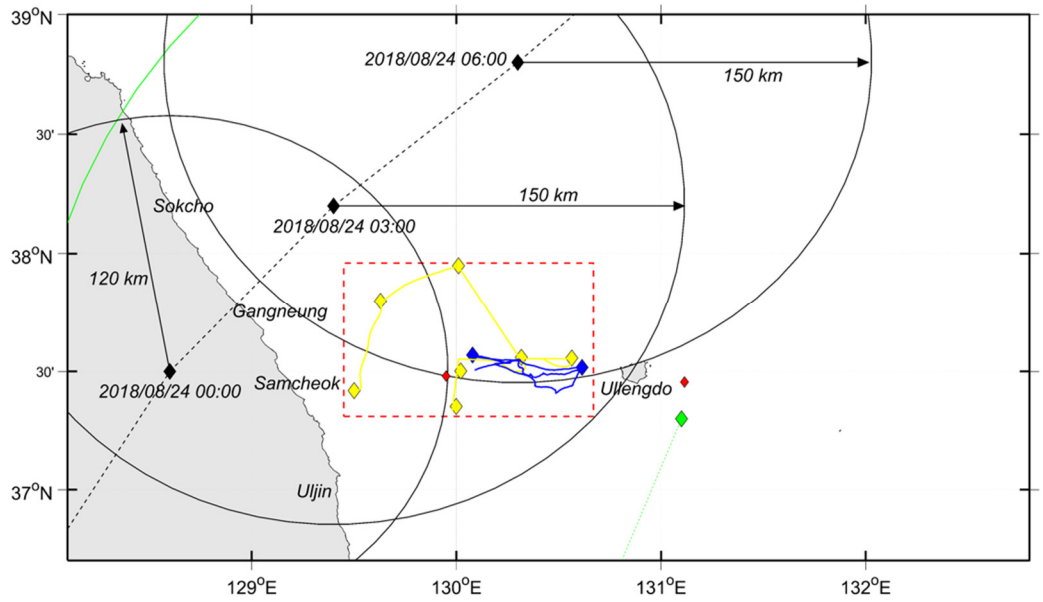

Fig. 6 Overview of the survey area

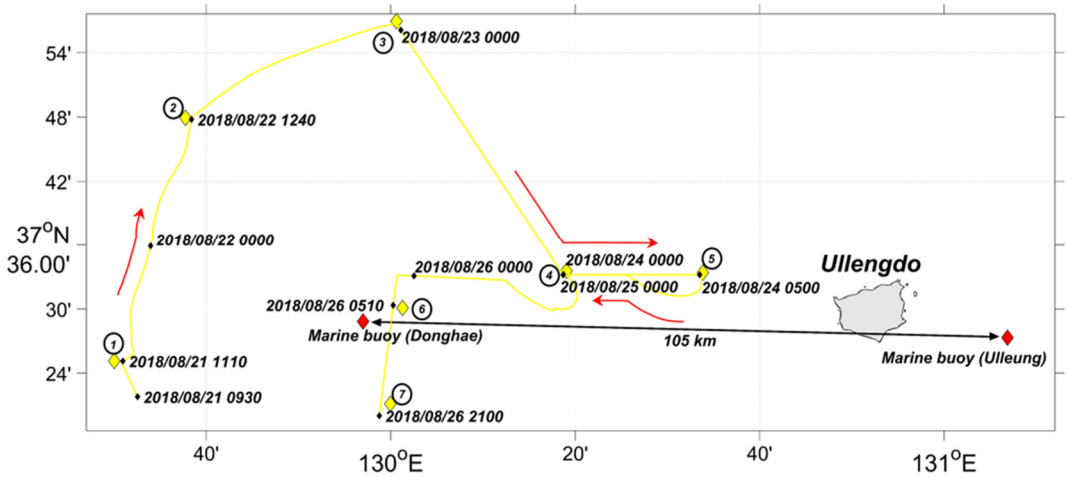

Fig. 7 Trajectory of the wave glider

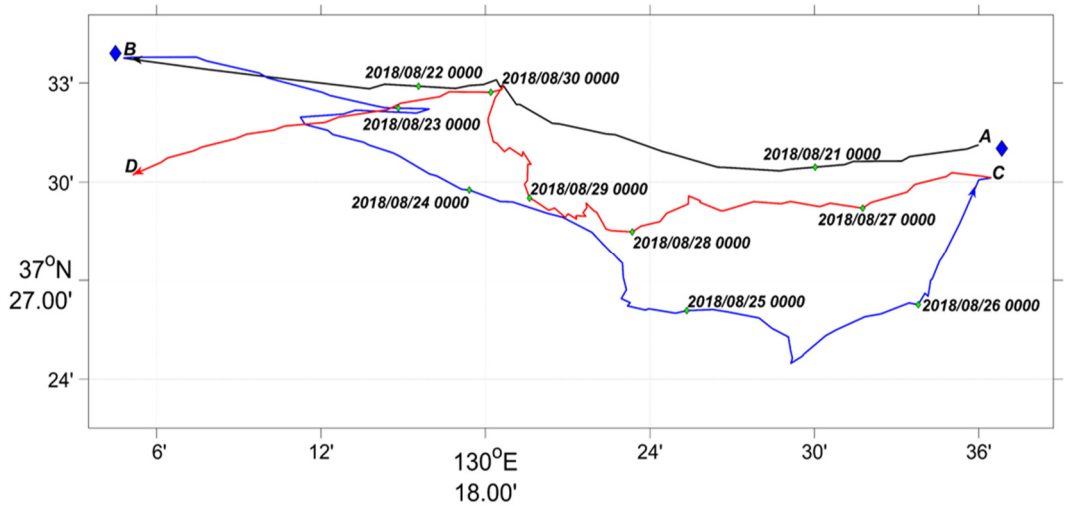

Fig. 8 Trajectory of the underwater glider

Fig. 7 and Fig. 8 illustrate the waypoints and trajectories of the wave and underwater gliders, respectively. The Donghae marine buoy was located within the survey area, while the Ulleung marine buoy was positioned outside, approximately 105 km away from the Donghae marine buoy. The marine buoys remained stationary, while the wave glider conducted an ocean survey following the designated waypoints. Table 2 shows the distances between each waypoint of the wave glider and the

marine buoys (Donghae and Ulleung). The wave glider was launched from the vicinity of Samcheok, traveling along waypoints 1 to 7. On the other hand, the underwater glider was launched near Ulleungdo, moving from east to west along the waypoints. Fig. 7 and Fig. 8 depict the wave glider following approximately straight lines between waypoints, while the underwater glider navigated by circumventing them.

Table 2 Distances between wave glider waypoints and marine buoys (Donghae and Ulleung)

	No. 1	No. 2	No. 3	No. 4	No. 5	No. 6	No. 7
Marine buoy (Donghae)	40	45	53	34	55	7	15
Marine buoy (Ulleung)	144	138	113	72	50	98	101

3.2. Meteorological data

Fig. 9 presents a graph comparing weather data obtained from a wave glider with a marine buoy and PacIOOS. Fig. 9 shows the dates when the waypoints (black dashed vertical lines and numbers) were passed, as well as the dates when typhoon Soulik passed through the East Sea and dissipated (green solid and dashed vertical lines). Due to weather sensor issues during the wave glider's ocean survey, only data until August 26 was utilized.

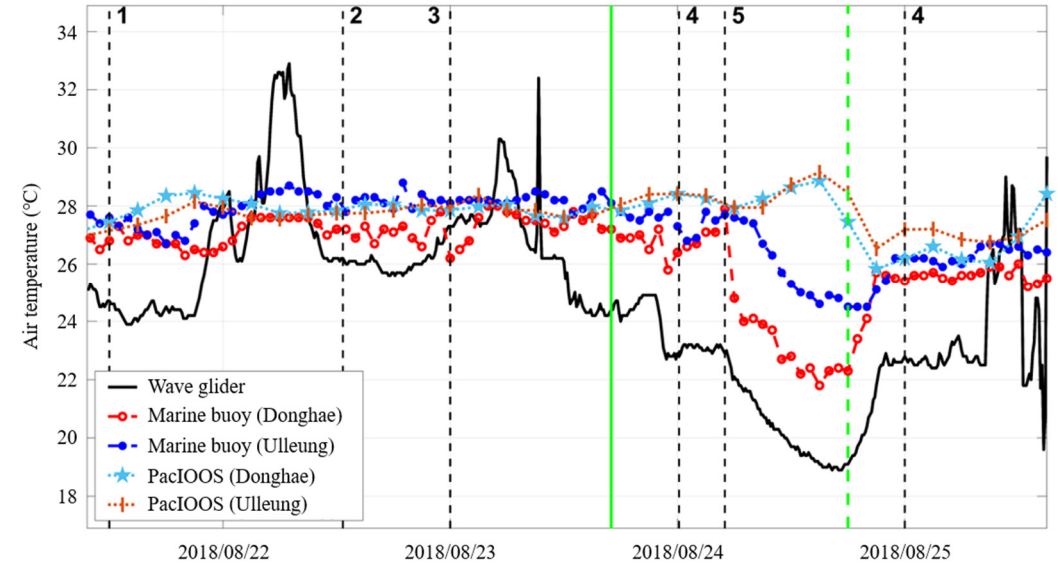

(a) Air temperature

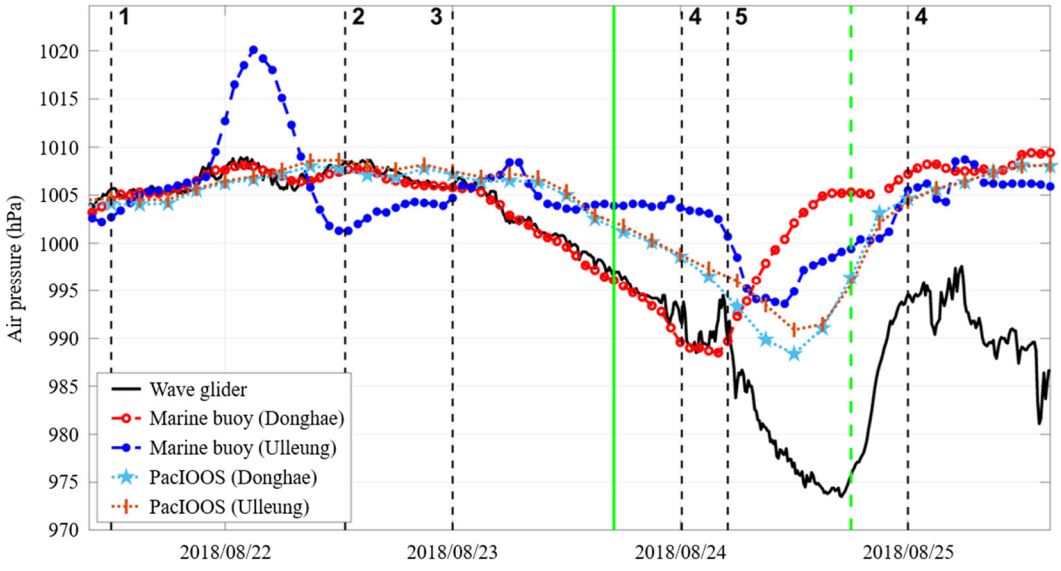

(b) Air pressure

Fig. 9 Meteorological observations of wave glider, marine buoy, and PacIOOS

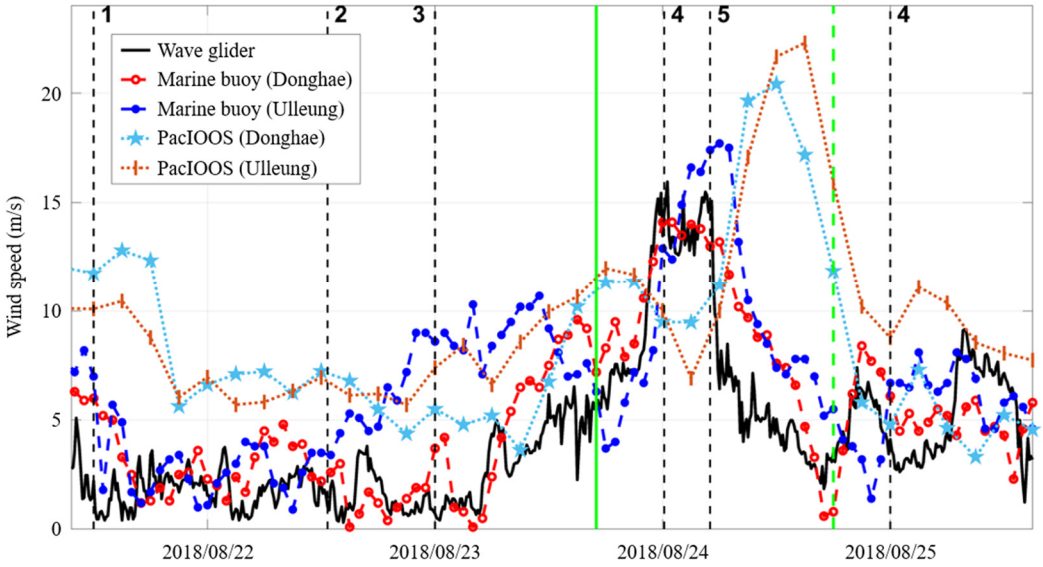

(c) Wind speed

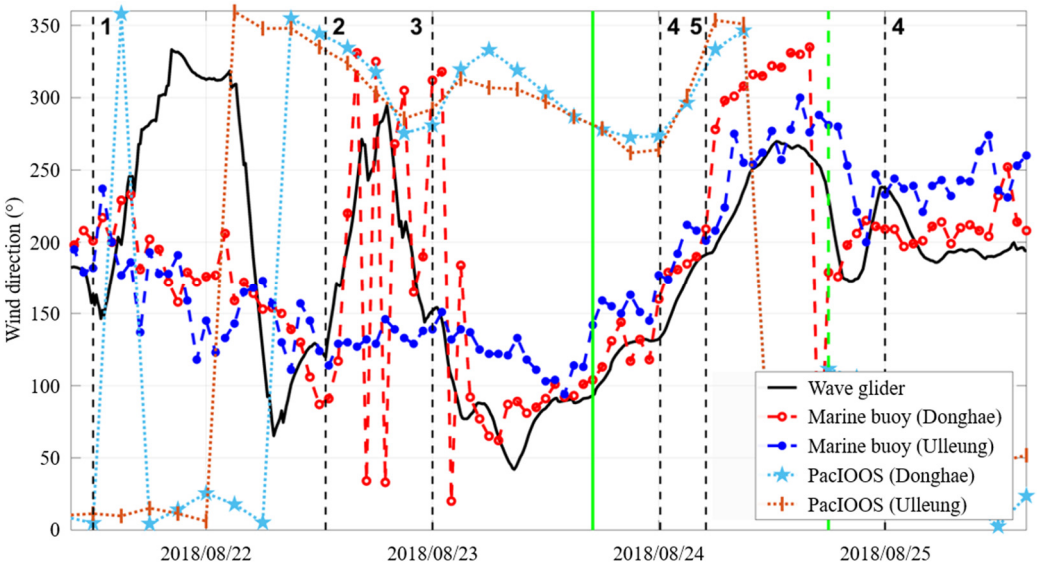

(d) Wind direction

Fig. 9 Meteorological observations of wave glider, marine buoy, and PacIOOS (continued)

In Fig. 9(a), temperature trends are depicted, with wave glider observations showing a rapid temperature increase from around 25 ℃(baseline) to over 30 ℃ twice until August 24, 0900 UTC (No. 4). Subsequently, after August 24, 1400 UTC (No. 5), there is a gradual decrease followed by an increase. Marine buoy and PacIOOS data exhibit a stable temperature trend around an average of 26 ℃ until No. 5. After No. 5, the two datasets showed different patterns. The marine buoy indicated a trend of decreasing followed by increasing temperatures, while PacIOOS data showed the opposite trend.

Fig. 9(b) illustrates the atmospheric pressure graph. The wave glider data reveals a gradual decrease in pressure from August 23, 0000 UTC, sharply dropping after No. 5 to a minimum of approximately 973.6 hPa. Even after the typhoon dissipated, the pressure continued to decrease before exhibiting an increasing trend. The Donghae marine buoy showed a similar trend to the wave glider data until No. 5, decreasing to around 990 hPa. However, unlike the wave glider data, it showed an increasing trend after No. 5. PacIOOS data also exhibited a similar decreasing trend after August 23, 0000 UTC, reaching a minimum (around 990 hPa) by August 24, 2100 UTC, and then showing an increasing trend.

Fig. 9(c) represents the wind speed graph. The wave glider data recorded increasing wind speeds from August 23, peaking at 15.95 m/s at 0910 UTC on August 24 (No. 4). After No. 5, the wind speed started decreasing, continued even after the typhoon was gone, and then picked up again about 7 hours later. The Donghae marine buoy data followed a similar pattern to

the wave glider, hitting a max wind speed of 14.1 m/s at No. 4. The Ulleung marine buoy recorded a max wind speed of around 17.7 m/s at No. 5 then decreased. PacIOOS data showed higher max wind speeds compared to the wave glider and the marine buoy, confirming they occurred after the typhoon had passed.

Fig. 9(d) represents the wind direction graph. The data observed by the wave glider showed two abrupt changes before 1800 UTC on August 23, gradually shifting clockwise from the time the typhoon entered the East Sea until its dissipation on August 25. The data from the Donghae and Ulleung marine buoys exhibited a similar trend with wind direction changing clockwise during a comparable period. In contrast, the PacIOOS wind direction results primarily pointed north, indicating no specific trend in that area.

3.3. CTD data

Fig. 10 depicts the vertical profile of water temperature up to a depth of 200 m over time. The white solid and dashed vertical lines represent the time when typhoon Soulik passed through the East Sea and dissipation, respectively. Fig. 10(a) reveals a mixed layer up to approximately 30 m, and depending on the period, a thermocline is present, ranging from a minimum of 80 m to over 200 m. From August 23, 1230 UTC, to August 26, noticeable variations in water temperature are observed not only in the surface layer but also in the 50 to 100 m depth range. After August 26, there is a general trend of decreasing temperatures observed down to a depth of 100 meters. In contrast, Fig. 10(b) does not exhibit subtle variations over time, forming a specific temperature gradient in the subsurface layer that remains relatively constant from August 23, 1230, UTC, to August 26, differing from the observed pattern in the underwater glider data.

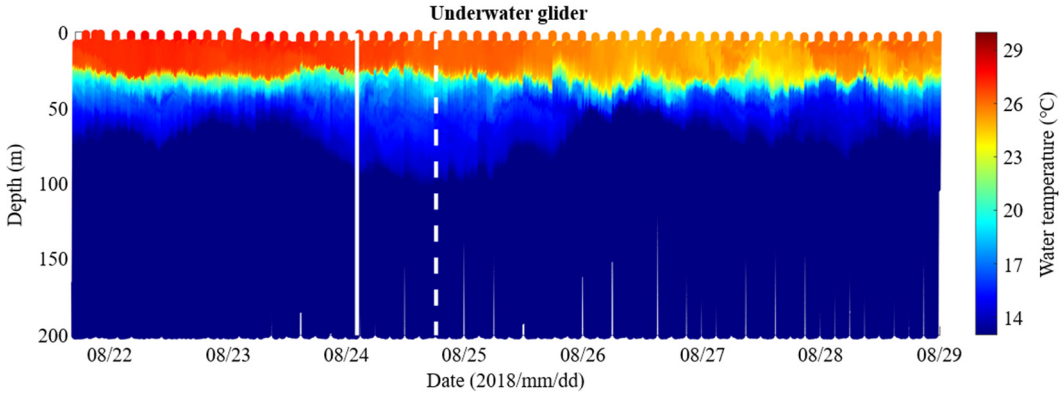

(a) Underwater glider

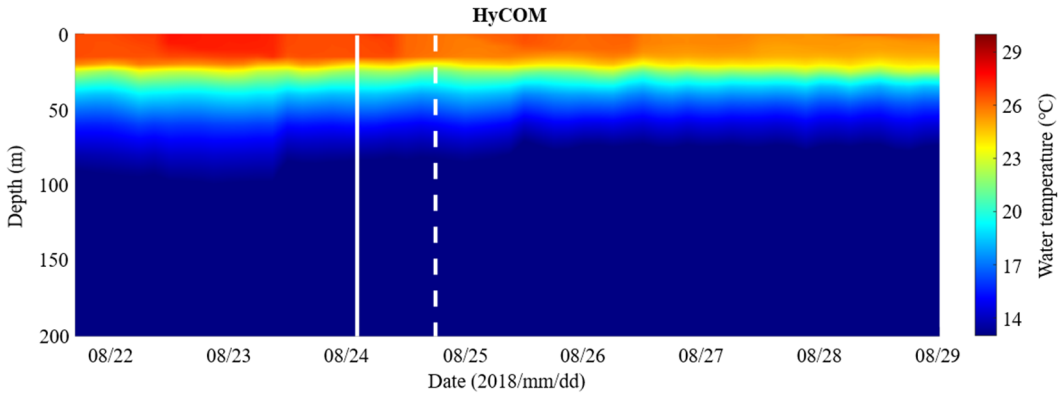

(b) HyCOM

Fig. 10 Comparing the water temperature response

Fig. 11 illustrates the vertical profile of salinity over time up to a depth of 200 m. From August 23, the salinity in the 0 to 50 m depth range, in Fig. 11(a), consistently increased. Starting from August 24, changes in salinity began in the deeper depths (near 200 m), eventually affecting salinity at all depths. Subsequently, as time progressed beyond August 26, salinity in depths deeper than 50 m gradually exhibited a distribution similar to the initial pattern.

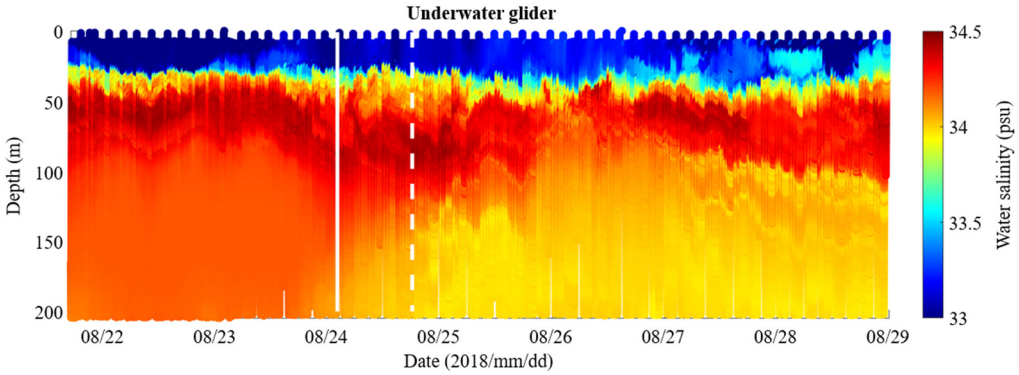

(a) Underwater glider

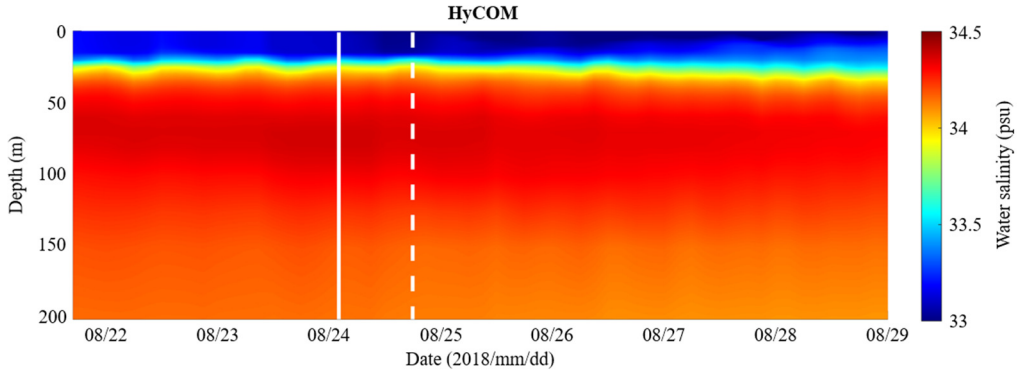

(b) HyCOM

Fig. 11 Comparing the water salinity response

Conversely, the HyCOM results, as depicted in Fig. 10(b), show a steady salinity gradient with minimal variations. Fig. 12 shows the vertical temperature profiles for two days before and after August 24, when the typhoon passed. Based on the data from August 24, the temperature distribution exhibited two distinct trends. Before the typhoon's passage, the temperature was elevated at the surface but began to decrease sharply at a depth of 20 m, falling below the temperature recorded on the 24th. At approximately 100 m depth, the temperature stabilized around 7 ℃ and was higher than the temperature on the 24th at depths greater than 140 m. However, after the typhoon passed, the surface temperature was relatively lower but remained elevated to a depth of 30 m, resulting in higher temperatures in the 20-40 m range. Below 40 m, the temperature was lower than that observed on the 24th, and no reversal of this trend was detected. The temperature gradually decreased to around 1 ℃ at a depth of 200 m.

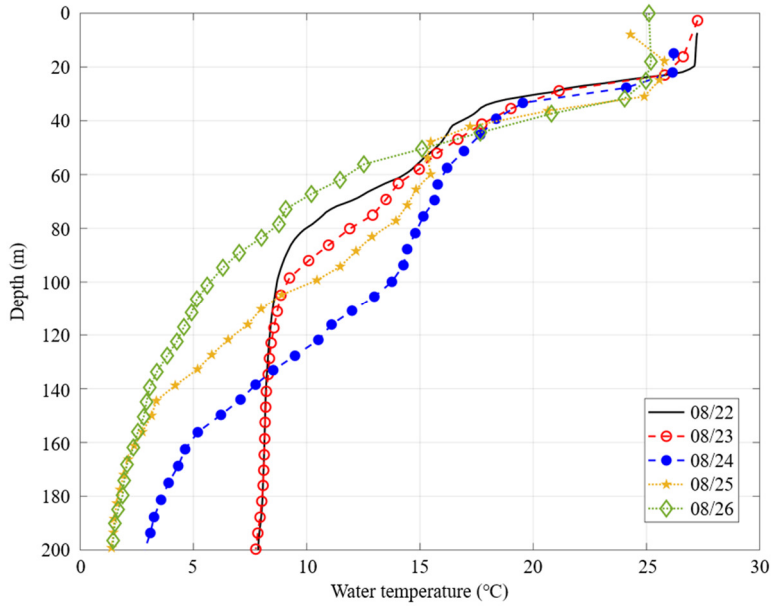

Fig. 12 Vertical profile of water temperature from August 22 to August 26

4. Discussion

Unmanned platforms used for oceanographic surveys require various operational capabilities, such as efficient transit to designated observation sites, utilizing a diverse selection of sensors to fulfill specific survey objectives, and ensuring the accuracy of the collected observational data. In this study, the straight-line transit performance of unmanned platforms to their respective waypoints was assessed. Additionally, the data from wave and underwater gliders were compared with marine buoy and forecast model data using root mean square error (RMSE) and correlation coefficients. Due to the high frequency of observations from the wave glider, which results in an extensive dataset, only data recorded at 1-hour intervals were used to match the marine buoy and PacIOOS forecast model data.

4.1. Movement performance of the unmanned platform

External factors such as wind, waves, and currents can impact the movement of both wave and underwater gliders. According to Chang et al. [24], as demonstrated through multi-body dynamics simulations in ADAMS software, the average propulsion speed of wave-powered vehicles tends to increase with a higher World Meteorological Organization (WMO) sea state code, particularly from No. 1 to 4. In environments with a sea state code of 3 or higher, the wave glider demonstrated excellent mobility by moving approximately in a straight line between waypoints. On the contrary, the underwater glider navigated by circumventing and occasionally moving backward. The underwater glider lacks its propulsion system, resulting in a movement speed of approximately 0.4-0.6 m/s and being susceptible to the influence of currents, as it operates exclusively underwater. Consequently, when the current speed exceeds that of the underwater glider, it impacts the mobility, as depicted in Fig. 8. While equipping a propeller can address this limitation, it introduces potential issues with operational time reduction, necessitating careful consideration of user objectives.

4.2. Comparison of meteorological data

Firstly, based on data from the KMA, when typhoon Soulik entered the East Sea, the central pressure was around 985 hPa, and the highest wind speed was about 22 m/s on August 24 at 0100 UTC. As a result, there's an issue with connecting the notable pressure drop shown by the wave glider in Fig. 9(b) solely to the typhoon's impact after No. 5. The investigation uncovered that the pressure port in the weather sensor might get blocked by salt crystals, causing inaccurate pressure readings. A clear indication of such occurrences is when the pressure oddly aligns with the temperature reading.

Therefore, the temperature and pressure data observed by the wave glider after No. 5 are unreliable. In Fig. 9(c) and Fig. 9(d), there are notable changes in wind speed and direction from August 23 until August 25, a trend not observed in other intervals. This suggests that the typhoon's strong wind radius is extensive, thus impacting weather conditions within the observation area even before the typhoon enters the East Sea. Summarizing Fig. 9, weather conditions within the observation area began to be influenced by the typhoon from 1200 UTC on August 23. During this period, atmospheric pressure gradually decreased, while wind speed increased. It is noteworthy that, after the point of the typhoon's dissipation, weather conditions returned to their original state. Additionally, the wind direction exhibited a gradual clockwise shift, indicating observations within the typhoon's danger quadrant. Overall, these findings provide a comprehensive illustration of the typhoon's characteristics.

Table 3 presents the correlation coefficients and RMSE values for marine buoy and PacIOOS data based on wave glider observational data. As shown in Fig. 9(a), the air temperature observed by the wave glider exhibited a lower temperature distribution compared to other datasets. Marine buoy and PacIOOS data generally showed similar trends; however, from No. 5 to No. 4, while the marine buoy data aligned with the wave glider observations, the PacIOOS data displayed differing results. This discrepancy resulted in an error of over 2 ℃ between the wave glider and PacIOOS data, affecting the correlation

coefficient. Regarding atmospheric pressure, the Donghae marine buoy data were consistent with the wave glider observations until No. 5, after which they exhibited opposite trends. Overall, the forecast model data showed a similar trend to the wave glider, while the Ulleung marine buoy data demonstrated no significant correlation. Consequently, the forecast model results displayed lower errors and higher correlations compared to the wave glider data.

Table 3 Comparison of the correlations of wave glider meteorological data with values from marine buoys and PacIOOS

Wave glider vs		Marine buoy (Donghae)	Marine buoy (Ulleung)	PacIOOS (Donghae)	PacIOOS (Ulleung)
Corr. Coef. (R)	Air temperature (℃)	0.794	0.793	0.066	-0.203
	Air pressure (hPa)	0.293	0.610	0.767	0.805
	Wind speed (m/s)	0.826	0.589	0.166	0.174
	Wind direction (°)	0.550	0.418	-0.566	-0.524
RMSE	Air temperature (℃)	2.506	3.359	4.230	4.346
	Air pressure (hPa)	11.884	11.107	9.204	9.474
	Wind speed (m/s)	2.324	4.011	6.530	7.219
	Wind direction (°)	67.921	70.474	184.794	182.996

However, data post-No. 5 are deemed invalid, suggesting that earlier data might have revealed different patterns. In Fig. 9(c), wind speed data from the marine buoy showed similar trends to the wave glider, with lower errors and higher correlation. In contrast, the forecast model exhibited excessive values and a delayed peak, leading to higher errors and lower correlation. For wind direction, marine buoy data generally aligned with the wave glider observations, showing correlations around 0.5 and lower errors.

Although the forecast model results appeared anomalous, this issue arose due to abrupt changes at certain intervals when angles exceeded 360° and wrapped around to 0°, affecting the representation of wind direction. Errors were predominantly opposite to the wave glider observations, resulting in negative correlation coefficients; however, similar values to the marine buoy data indicated a maintained association. Peng et al. [25] noted that the forecast model tends to overestimate wind strength in the typhoon boundary layer when U10 exceeds 10 m/s. The model's performance appears to degrade when wind flows originate from the land-sea boundary, and the reliability of simulated wind speeds diminishes as proximity to the typhoon's center increases. This observation suggests potential causes for the errors in wind speed and direction results.

4.3. Comparison of CTD data

In Fig. 10(a), the water temperature exhibited an increasing trend from August 23, 1200 UTC, before the typhoon entered the East Sea. The temperature rose to a depth of approximately 100 m and gradually decreased after the typhoon dissipated, returning to the previous temperature distribution by August 26. Similarly, in Fig. 11(a), changes in salinity distribution began around August 23, 1200 UTC. Initially, there was an increasing trend in the upper layers, but after August 24, a simultaneous decrease in salinity from a depth of 200 m was observed. While data below 200 m is unavailable, there is a possibility of salinity changes at greater depths. Unlike water temperature, salinity tends to return to the previous distribution after August 26, but complete recovery was not observed during the observation period.

Combining Fig. 9 through Fig. 12, the characteristics of typhoon-induced changes in wind direction, wind speed, and sea surface vertical mixing can be observed during the typhoon passage. The impact on water temperature and salinity distribution is evident. The trends observed in Fig. 10 and Fig. 11, particularly the vertical profiles of temperature and salinity, are consistent with the vertical mixing patterns identified by Wang et al. [26] in their study. This suggests that vertical mixing likely played a significant role in the observed changes. While meteorological data typically return to pre-typhoon conditions within several hours to days, sea surface marine properties generally recover to their original values within several days to weeks [27-28]. The subsurface ocean layers, which have limited contact with the atmosphere, tend to recover more slowly. Therefore, the deep-layer salinity may require a longer time to return to its initial state, which was not observed in Fig. 11(a).

The forecast model results, in the case of PacIOOS, show some differences compared to observational data but still exhibit a certain level of trend. On the other hand, the HyCOM calculations were challenging to compare comprehensively with the submersible glider data. A major factor contributing to these differences can be attributed to the availability of basic data. While meteorological data can benefit from unmanned observation equipment covering the globe, marine data acquisition is limited to specific regions, resulting in relatively insufficient data. Consequently, in marine cases where observational data is lacking, accuracy in results tends to be lower.

Moreover, to align with computer specifications, calculations involve setting a minimum temporal and spatial resolution of 1 hour and several kilometers, respectively, making it difficult to capture subtle changes observed in the data. To overcome the mentioned challenges, improving calculation methods or computer performance is practically difficult. Therefore, efforts are underway to obtain a substantial amount of foundational data by conducting direct human surveys or utilizing various marine equipment such as satellites, Argo floats, buoys, etc., aiming to acquire global meteorological and oceanic data. In this study, unmanned platforms like wave gliders and underwater gliders were employed. As seen in Fig. 9 to Fig. 11, these autonomous platforms can acquire high-resolution spatiotemporal data, complementing the limitations of the equipment mentioned above.

5. Conclusions

This study utilized unmanned platforms, specifically wave and underwater gliders, to investigate the impact of typhoon Soulik on the marine environment in the East Sea. The primary objective was to understand the changes in weather and marine conditions before and after the typhoon and to evaluate the effectiveness of unmanned platforms in marine surveys. From August 20 to 30, 2018, wave and underwater gliders collected meteorological and CTD data in the area affected by the typhoon. The collected data were compared with marine buoy and forecast model data using RMSE and correlation coefficients for analysis. The results of the study are as follows.

(1) The data collected by the unmanned platforms effectively represented changes in the marine environment during the typhoon, with vertical mixing identified as a significant mechanism in constructing vertical temperature profiles.

(2) The comparison of data revealed the characteristics of each observational tool. Marine buoys provide precise data but are limited to fixed points, requiring numerous buoys for comprehensive coverage. In contrast, forecast models offer broad spatial coverage but may yield less accurate results due to computational constraints.

(3) Limitations of the study include the difficulty in obtaining specialized forecast model data for the Korean region and the lack of buoy data in offshore areas, which posed challenges for comparison.

Future research should aim to enhance the study's scope by employing diverse methodological approaches to collect marine environmental data across various settings and by developing advanced clustering systems. Additionally, improving the accuracy of forecast models will be crucial. This study demonstrates that unmanned platforms can effectively operate in extreme weather and inaccessible areas, providing valuable data without temporal and spatial constraints. It emphasizes the need for high-quality foundational data to improve the accuracy of forecast models. These platforms hold the potential for advancing marine research and enhancing forecast model precision.

Funding

This research was supported by the Unmanned Vehicles Core Technology Research and Development Program through the National Research Foundation of Korea (NRF) and the Unmanned Vehicle Advanced Research Center (UVARC), funded by the Ministry of Science and ICT, the Republic of Korea (NRF-2020M3C1C1A02086324).

Conflicts of Interest

The authors declare no conflict of interest.

References

[1] R. Hine, S. Willcox, G. Hine, and T. Richardson, "The Wave Glider: A Wave-Powered Autonomous Marine Vehicle," OCEANS 2009, pp 1-6, October 2009.

[2] J. Manley and S. Willcox, "The Wave Glider: A Persistent Platform for Ocean Science," OCEANS'10 IEEE SYDNEY, pp. 1-5, May 2010.

[3] P. Carragher, G. Hine, P. Legh-Smith, J. Mayville, R. Nelson, et al., "A New Platform for Offshore Exploration and Production," Oilfield Review Winter 2013/2014, vol. 25, no. 4, pp. 40-50, 2014.

[4] J. Mullison, D. Symonds, and N. Trenaman, "ADCP Data Collected From a Liquid Robotics Wave Glider," IEEE/OES 10th Current, Waves and Turbulence Measurements, pp. 266-272, March 2011.

[5] P. J. Bresnahan, T. Wirth, T. R. Martz, A. J. Andersson, T. Cyronak, S. D'Angelo, et al., "A Sensor Package for Mapping pH and Oxygen From Mobile Platforms," Methods in Oceanography, vol. 17, pp. 1-13, December 2016.

[6] J. Thomson and J. Girton, "Sustained Measurements of Southern Ocean Air-Sea Coupling from a Wave Glider Autonomous Surface Vehicle," Oceanography, vol. 30, no. 2, pp. 104-109, June 2017.

[7] T. Moh, J. H. Cho, S. K. Jung, S. H. Kim, and Y. B. Son, "Monitoring of the Changjiang River Plume in the East China Sea Using a Wave Glider," Journal of Coastal Research, no. 85, pp. 26-30, May 2018.

[8] S. Wiggins, J. Manley, E. Brager, and B. Woolhiser, "Monitoring Marine Mammal Acoustics Using Wave Glider," OCEANS 2010 MTS/IEEE SEATTLE, pp. 1-4, September 2010.

[9] J. M. Wilson, R. Severson, and J. M. Beman, "Ocean-Scale Patterns in Community Respiration Rates Along Continuous Transects Across the Pacific Ocean," Plos One, vol. 9, no. 7, article no. e99821, 2014.

[10] S. Mitarai and J. C. McWilliams, "Wave Glider Observations of Surface Winds and Currents in the Core of Typhoon Danas," Geophysical Research Letters, vol. 43, no. 21, pp. 11,312-311,319, November 2016.

[11] J. Sherman, R. E. Davis, W. Owens, and J. Valdes, "The Autonomous Underwater Glider "Spray"," IEEE Journal of Oceanic Engineering, vol. 26, no. 4, pp. 437-446, October 2001.

[12] R. Bachmayer, N. E. Leonard, J. Graver, E. Fiorelli, P. Bhatta, and D. Paley, "Underwater Gliders: Recent Developments and Future Applications," Proceedings of the 2004 International Symposium on Underwater Technology (IEEE Cat. No.04EX869), pp. 195-200, April 2004.

[13] B. Garau, S. Ruiz, W. G. Zhang, A. Pascual, E. Heslop, J. Kerfoo, et al., "Thermal Lag Correction on Slocum CTD Glider Data," Journal of Atmospheric and Oceanic Technology, vol. 28, no. 9, pp. 1065-1071, September 2011.

[14] M. Zhou, R. Bachmayer, and B. deYoung, "Towards Autonomous Underwater Iceberg Profiling Using a Mechanical Scanning Sonar on a Underwater Slocum Glider," IEEE/OES Autonomous Underwater Vehicles, pp. 101-107, November 2016.

[15] N. D. Nguyen, H. S. Choi, H. S. Jin, J. Huang, and J. H. Lee, "Robust Adaptive Depth Control of Hybrid Underwater Glider in Vertical Plane," Advances in Technology Innovation, vol. 5, no. 3, pp. 135-146, July 2020.

[16] A. Kitamoto, "Digital Typhoon: Typhoon 201819 (SOULIK) - General Information (Pressure and Track Charts)," http://agora.ex.nii.ac.jp/digital-typhoon/summary/wnp/s/201819.html.en, February 02, 2024.

[17] R. N. Smith, J. Das, G. Hine, W. Anderson, and G. S. Sukhatme, "Predicting Wave Glider Speed From Environmental Measurements," OCEANS'11 MTS/IEEE KONA, pp. 1-8, September 2011.

[18] O. Schofield, J. Kohut, D. Aragon, L. Creed, J. Graver, C. Haldeman, et al., "Slocum Gliders: Robust and Ready," Journal of Field Robotics, vol. 24, no. 6, pp. 473-485, June 2007.

[19] P. Gemelli, P. M. Poulain, M. I. Zignego, and D. Cecchi, "Slocum Underwater Glider Acoustic Capabilities Improvement by Wings Re-Design," IMEKO TC-19 International Workshop on Metrology for the Sea, pp. 179-183, October 2019.

[20] K. Y. Oh, J. Y. Kim, J. S. Lee, and K. W. Ryu, "Wind Resource Assessment Around Korean Peninsula for Feasibility Study on 100 MW Class Offshore Wind Farm," Renewable Energy, vol. 42, pp. 217-226, June 2012.

[21] S. Park, J. S. Park, and T. R. Kim, "Trapped-Fetch Wave Model Application to Typhoon Case," Tropical Cyclone Research and Review, vol. 1, no. 3, pp. 390-401, September 2012.

[22] D. Partridge, T. Friedrich, and B. S. Powell, "Reanalysis of the PacIOOS Hawaiian Island Ocean Forecast System, an Implementation of the Regional Ocean Modeling System v3.6," Geoscientific Model Development, vol. 12, no. 1, pp. 195-213, 2019.

[23] E. P. Chassignet, H. E. Hurlburt, E. J. Metzger, O. M. Smedstad, J. A. Cummings, G. R. Halliwell, et al., "US GODAE: Global Ocean Prediction With the HYbrid Coordinate Ocean Model (HYCOM)," Oceanography, vol. 22, no. 2, pp. 64-75, June 2009.

[24] Z. Y. Chang, C. Deng, J. K. Zhang, Z. X. Feng, and Z. Q. Zheng, "Propulsion Performance Analysis of Wave-Powered Boats," International Journal of Engineering and Technology Innovation, vol. 10, no. 2, pp. 121-129, 2020.

[25] S. Peng, Y. Liu, R. Li, Y. Wei, P. W. Chan, S. Li, "Error Features in Predicting Typhoon Winds: A Case Study Comparing Simulated and Measured Data," Atmosphere, vol. 13, no. 2, article no. 158, February 2022.

[26] H. Wang, J. Li, J. Song, H. Leng, H. Zhang, X. Chen, et al., "Ocean Response Offshore of Taiwan to Super Typhoon Nepartak (2016) Based on Multiple Satellite and Buoy Observations," Frontiers in Marine Science, vol. 10, article no. 1132714, March 2023.

[27] K. Emanuel, "Contribution of Tropical Cyclones to Meridional Heat Transport by the Oceans," Journal of Geophysical Research: Atmosphere, vol. 106, no. D14, pp. 14771-14781, July 2001.

[28] G. Wang, L. Wu, N. C. Johnson, and Z. Ling, "Observed Three-Dimensional Structure of Ocean Cooling Induced by Pacific Tropical Cyclones," Geophysical Research Letters, vol. 43, no. 14, pp. 7632-7638, July 2016.